Physica A 392 (2013) 1762–1769

Contents lists available at SciVerse ScienceDirect

Physica A

journal homepage: www.elsevier.com/locate/physa

Some dynamical properties of a classical dissipative bouncing ball model with two nonlinearities

Diego F.M. Oliveira [a,b], Edson D. Leonel [c,*]

[a] Institute for Multiscale Simulation at the Friedrich Alexander Universität Erlangen-Nürnberg, Naegelsbachstrasse 49b, D-91052-Erlangen, Germany

[b] CAMTP - Center For Applied Mathematics and Theoretical Physics, University of Maribor, Krekova 2, SI-2000-Maribor, Slovenia

[c] Departamento de Física, UNESP - Univ Estadual Paulista, Av. 24A, 1515-13506-900-Rio Claro, SP, Brazil

ARTICLE INFO

Article history:
Received 30 November 2012
Available online 3 January 2013

Keywords:
Chaos
Fermi-map
Boundary crisis

ABSTRACT

Some dynamical properties for a bouncing ball model are studied. We show that when dissipation is introduced the structure of the phase space is changed and attractors appear. Increasing the amount of dissipation, the edges of the basins of attraction of an attracting fixed point touch the chaotic attractor. Consequently the chaotic attractor and its basin of attraction are destroyed given place to a transient described by a power law with exponent −2. The parameter-space is also studied and we show that it presents a rich structure with infinite self-similar structures of shrimp-shape.

1. Introduction

The origin of the high energy cosmic rays has intrigued the scientists during the first half of the 20th century. However, in 1949, Enrico Fermi [1], in his pioneering paper *On the origin of cosmic radiation*, proposed that a charged particle could be accelerated by iterations with time-dependent magnetic structures. Since then many different models were proposed in classical [2–9] and in quantum domains [10–14].

One of the models that has been considered very often in the literature is the Fermi–Ulam model (FUM), sometimes called as bouncing ball model. The system consists of a classical particle (denoting the cosmic ray) confined inside and bouncing between two rigid walls: one of them is moving periodically in time (corresponding to the moving magnetic field) while the other is fixed (returning mechanism of the particle towards a further collision with the moving wall). Despite the simplicity of the model, the non-dissipative dynamics of the problem has a very rich and complex phase space. Therefore depending on both the control parameters and initial conditions, regular regions such as invariant spanning curves (also known in theory of nonlinear dynamics as invariant tori) and Kolmogorov–Arnold–Moser (KAM) islands are observed coexisting with chaotic seas. Contrary to what would be expected by the collisions with the moving wall, Lichtenberg and Lieberman [15] showed that the existence of a set of invariant tori in the phase space prevent the particle to accumulate unlimited energy. However, searching for conditions to produce the unlimited energy growth of the bouncing particle, Leonel and Silva [16] in 2008 proposed a specific type of external perturbation of the wall that, depending on the range of control parameters, the growth in the particle's energy was observed. Indeed they considered that the moving wall is connected to a crank by a rod. Therefore for such a system, there are two nonlinearities in the dynamics playing important roles in the velocity of the particle. When the length of the crank approaches the limit of the length of the rod, the motion of the moving wall becomes very fast for certain phases leading the velocity of the wall to become discontinuous for such phases leading to large jumps in the particle velocity and hence to unlimited energy growth. Before such a limit however, the phase space experiences abrupt destruction of invariant tori due to parameter changes leading to merging and overlaps of different chaotic seas.

* Corresponding author. Tel.: +55 1935269174.
E-mail addresses: diegofregolente@gmail.com (D.F.M. Oliveira), edleonel@rc.unesp.br (E.D. Leonel).

0378-4371/$ – see front matter © 2013 Elsevier B.V. All rights reserved.
doi:10.1016/j.physa.2012.12.021

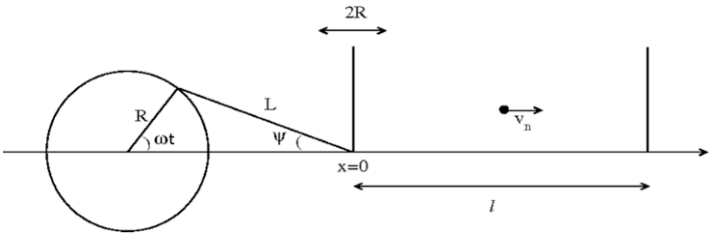

Fig. 1. Illustration of the model.

In this paper we revisit the problem proposed in Ref. [16] seeking to understand and describe some dissipative properties of the dynamics. Thus the model consists of a classical particle confined between two rigid walls. One wall is fixed and the other one moves periodically in time. We assume that the particle experiences inelastic collisions with both walls leading to a fractional loss of energy upon collision. For the fixed wall, we introduce a coefficient $\alpha \in [0, 1]$ while for the periodically varying wall we consider $\beta \in [0, 1]$. The limit $\alpha = \beta = 1$ recovers the results for the non dissipative case. We describe the dynamics via a two dimensional non-linear area-contracting map with four effective control parameters namely: two dissipation parameters and two parameters controlling the nonlinearity of the system. We show that the introduction of dissipation destroys the mixed structure of the phase space. A direct conclusion is that elliptical fixed points turn into sinks and the chaotic sea can be replaced by a chaotic attractor [17]. Each of these structures have their own basin of attraction. When the amount of the dissipation is increased, the edges between the basin of attraction of the attracting fixed point and of the basin of attraction of the chaotic attractor[1] touch the unstable manifold[2] and as a result the chaotic attractor as well as its basin of attraction are suddenly destroyed. Such an event is called boundary crisis [17–19]. After the destruction, the chaotic attractor is replaced by a transient which is characterized by a power law where the independent coordinate is the relative distance, in the control parameter, where the crisis takes place.

Dissipative systems have attracted much attention during the last decades, not only in order to characterize boundary crisis but also because they can be applied in turbulent dynamics [20], molecular physics [21] and many other fields. In the field of Fermi acceleration (FA), it has been shown that the introduction of dissipation works as a mechanism for the suppression of the unlimited energy growth [22–26]. Attention also has been devoted to the parameter space of the dissipative systems. In particular much interest is applied in order to investigate the existence of structures called *shrimps* [27], as reported by Gallas in Ref. [27] in 1993. Since then and considering the advances of fast computers, the parameter-space of dissipative models has received special attention and extensive works have been done not only in theoretical models [28–34] (and references therein) but also very recently the existence of shrimp-shaped domains experimentally involving a circuit of the Nishio–Inaba family [35] has been shown. Here, we have used Lyapunov exponents to classify regions in the parameter-space as regular (null or negative Lyapunov exponent) or chaotic behavior (positive Lyapunov exponent). The procedure we have adopted is: starting with a fixed initial condition, for each increment in the parameters we follow the attractor. This means that we use the last value obtained for the dynamical variables before the increment, as the new initial condition after the increment and we show that the parameter space exhibits a shrimp shade structure which corresponds to the periodic attractors embedded in a chaotic region.

The present paper is organized as follows. In Section 2 we describe all the necessary details to obtain the two-dimensional mapping that describes the dynamics of the system. Moreover, our numerical results for the boundary crisis and shrimp-shape structures are shown along the section. Finally, conclusions are drawn in Section 4.

2. A dissipative Fermi–Ulam model with two nonlinearities

In this section we revisit the model introduced by Leonel and Silva in 2008 [16], however, here, the dissipative dynamics is taken into account. We begin describing the problem and the steps necessary to construct the mapping. The model consists of a classical particle confined between two rigid walls. One of them is considered to be fixed at $x = l$ while the other one is connected in a crank by a rod with length L and it moves periodically in time according to $x_w(t) = R\cos(\omega t) + \sqrt{L^2 - R^2\sin^2(\omega t)} - L$, constructed from the center of the circle, where R is the radius of the crank (the amplitude of oscillation) and ω is the frequency as one can see in Fig. 1. The particle is in the complete absence of any external field. We assume that collisions with both walls are inelastic. Thus, the restitution coefficient $\beta \in [0, 1)$ is introduced when the particle hits the periodically time varying wall. On the other hand, in collisions with the fixed wall, the coefficient $\alpha \in [0, 1)$ is assumed. We take into account values for both α and β inside the interval $(0, 1)$. The dynamics of the system is described in terms of a two dimensional non-linear area-contracting map for the variables velocity and time. Thus, it is convenient to define some dimensionless variables. The time is measured in terms of the number of oscillations of the moving wall,

[1] The edges correspond indeed to the stable and unstable manifolds of a saddle fixed point. They are obtained by using the inverse of the map.

[2] Chaotic attractor.

consequently $\phi_n = \omega t_n$. A dimensionless velocity is given by $V_n = v_n/(\omega l)$, $\epsilon = R/l$ and $r = R/L$. Thus, the two-dimensional map $T(V_n, \phi_n) = (V_{n+1}, \phi_{n+1})$ that describes the dynamics of the system is given by

$$T : \begin{cases} V_{n+1} = V_n^* - (1+\beta)\epsilon \sin(\phi_{n+1}) \left[1 + \dfrac{r\cos(\phi_{n+1})}{\sqrt{1 - r^2\sin^2(\phi_{n+1})}} \right], \\ \phi_{n+1} = [\phi_n + \Delta T_n] \bmod (2\pi) \end{cases} \tag{1}$$

where the corresponding expressions for both V_n^* and ΔT_n depend on what kind of collision occurs, namely: (i) successive collisions and; (ii) non-successive collisions. The successive collisions happen when the particle enters the collision zone, $x \in [-\epsilon, \epsilon]$, experiences a collision with the moving wall, and before it leaves the collision zone, it experiences a second, and therefore successive collision. Additionally, depending on the combination of both, velocity and phase, many collisions may happen before the particle leaves the collision zone. In case (i), the corresponding expressions for both V_n^* and ΔT_n are given by $V_n^* = -\beta V_n$ and $\Delta T_n = \phi_c$. The numerical value of ϕ_c is obtained as the first solution of the equation $G(\phi_c) = 0$ with $\phi_c \in (0, 2\pi]$. Where the function $G(\phi_c)$ is obtained by the condition that the position of the particles is the same as that of the wall. Thus, $G(\phi_c)$ is then written as

$$G(\phi_c) = \epsilon\cos(\phi_n + \phi_c) + \frac{\epsilon}{r}\sqrt{1 - r^2\sin^2(\phi_n + \phi_c)} - \epsilon\cos(\phi_n) - \frac{\epsilon}{r}\sqrt{1 - r^2\sin^2(\phi_n)} - V_n\phi_c. \tag{2}$$

If the function $G(\phi_c)$ does not have a solution in the interval $\phi_c \in (0, 2\pi]$, one must conclude that the particle leaves the collision zone without experiencing a successive collision. It is easy to show that the determinant of the Jacobian matrix for the mapping which describes the case of successive collisions is given by

$$\det(J) = \beta^2 \left[\frac{V_n + \epsilon\sin(\phi_n)\left(1 + \frac{r\cos(\phi_n)}{\sqrt{1-r^2\sin^2(\phi_n)}}\right)}{V_{n+1} + \epsilon\sin(\phi_{n+1})\left(1 + \frac{r\cos(\phi_{n+1})}{\sqrt{1-r^2\sin^2(\phi_{n+1})}}\right)} \right]. \tag{3}$$

Considering now the case of non-successive collisions, the expressions for both V^* and ΔT are $V_n^* = \beta\alpha V_n$ and $\Delta T_n = \phi_r + \phi_l + \phi_c$, where the auxiliary terms are written as

$$\phi_r = \frac{r[1 - \epsilon\cos(\phi_n)] - \epsilon\sqrt{1 - r^2\sin^2(\phi_n)} - \epsilon}{rV_n}, \qquad \phi_l = \frac{1-\epsilon}{\alpha V_n}. \tag{4}$$

Here ϕ_r denotes the time that the particle spends traveling to the right hand side until it hits the fixed wall. The particle thus experiences an inelastic collision and is reflected backwards with velocity $-\alpha V_n$. Then, the term ϕ_l denotes the time that the particle spends until entering again the collision zone. Finally, ϕ_c is numerically obtained as the smallest solution of the equation $F(\phi_c) = 0$ with $F(\phi_c)$ given by

$$F(\phi_c) = \epsilon\cos(\phi_n + \phi_r + \phi_l + \phi_c) + \frac{\epsilon}{r}\sqrt{1 - r^2\sin^2(\phi_n + \phi_r + \phi_l + \phi_c)} + \frac{\epsilon}{r}(1+r) + \alpha V_n\phi_c. \tag{5}$$

After some algebra, one can show that the determinant of the Jacobian matrix for the case of non-successive collisions is given by

$$\det(J) = \alpha^2\beta^2 \left[\frac{V_n + \epsilon\sin(\phi_n)\left(1 + \frac{r\cos(\phi_n)}{\sqrt{1-r^2\sin^2(\phi_n)}}\right)}{V_{n+1} + \epsilon\sin(\phi_{n+1})\left(1 + \frac{r\cos(\phi_{n+1})}{\sqrt{1-r^2\sin^2(\phi_{n+1})}}\right)} \right]. \tag{6}$$

It is clear that the above result implies that the model is measure preserving only for the case of both $\alpha = \beta = 1$.

In order to describe occurrence of homoclinic orbits, we must firstly know exactly the location of the saddle fixed points. Thus, in order to obtain the position of the fixed points we have to solve the equations $V_{n+1} = V_n$ and $\phi_{n+1} = \phi_n + 2m\pi$. The solutions of these equations give us that the saddle fixed points are written as

$$V = \left[\frac{1+\beta}{\beta\alpha - 1}\right]\epsilon\sin(\phi)\left[1 + \frac{r\cos(\phi)}{\sqrt{1 - r^2\sin^2(\phi)}}\right], \tag{7}$$

$$h(\phi) = 1 - \gamma\sin(\phi)\left[1 + \frac{r\cos(\phi)}{\sqrt{1 - r^2\sin^2(\phi)}}\right] - \epsilon\cos(\phi) - \frac{\epsilon}{r}\sqrt{1 - r^2\sin^2(\phi)}, \tag{8}$$

where ϕ is obtained numerically by solving $h(\phi) = 0$ by using Newton's method. The auxiliary term γ is defined as

$$\gamma = \frac{2\epsilon\alpha m\pi}{\alpha + 1}\left[\frac{1+\beta}{\beta\alpha - 1}\right], \tag{9}$$

and $m = 1, 2, 3, \ldots$.

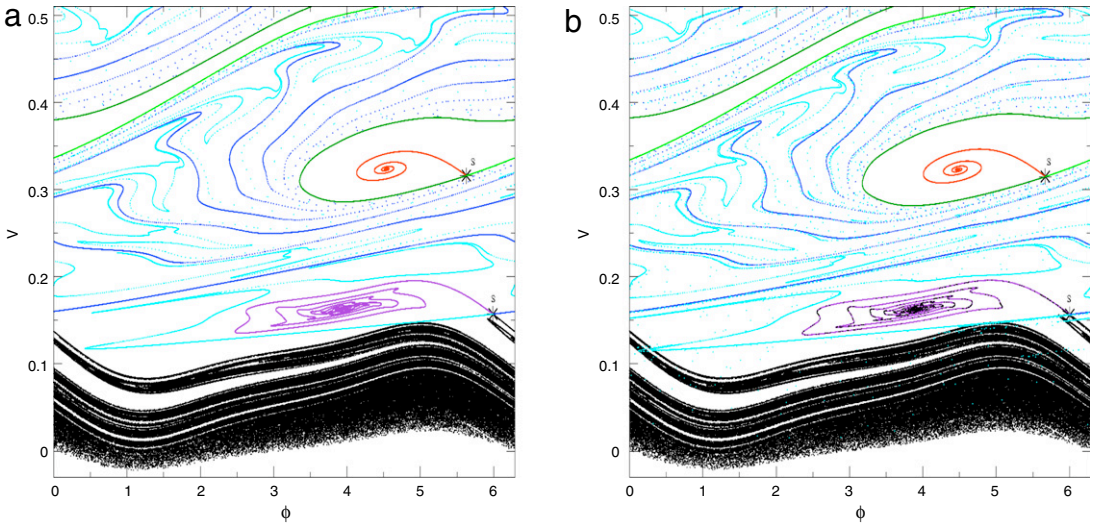

Fig. 2. Characterization of a boundary crisis for $m = 2$. The control parameters used were $\epsilon = 0.02$, $r = 0.5$, $\beta = 0.98$ and: (a) $\alpha = 0.91$ (immediately before the crisis); (b) $\alpha = 0.915$ (immediately after the crisis).

It is well known that a saddle fixed point (represented by a star in Fig. 2) has both stable and unstable manifolds. The unstable manifolds are obtained by trajectories heading directly to the attracting fixed points (upper branch) or approaching the chaotic attractor (lower branch) (see Fig. 2). They are obtained just via the iteration of the mapping T with the appropriate initial conditions. On the other hand, the stable manifolds consist basically of the boundary between the basin of attraction of the attracting fixed point and the basin of attraction of the chaotic attractor. The construction of the stable manifolds are slightly more complicated than the unstable manifolds, since we have to obtain the inverse of the mapping T. The basic procedure is that $T^{-1}(V_{n+1}, \phi_{n+1}) = (V_n, \phi_n)$, thus the expression of the velocity is given by

$$V_n = \frac{1}{\beta\alpha}\left[V_{n+1} + (1+\beta)\epsilon\,\sin(\phi_{n+1})\left[1 + \frac{r\cos(\phi_{n+1})}{\sqrt{1 - r^2\sin^2(\phi_{n+1})}}\right]\right]. \tag{10}$$

The phase ϕ_n is obtained from the condition $K(\phi_n) = 0$, where $K(\phi_n)$ is written as

$$K(\phi_n) = (\phi_n - \phi_{n+1})\left[V_{n+1} + (1+\beta)\epsilon\,\sin(\phi_{n+1})\left(1 + \frac{r\cos(\phi_{n+1})}{\sqrt{1 - r^2\sin^2(\phi_{n+1})}}\right)\right]$$
$$+ \beta(1+\alpha) - \epsilon\beta[\alpha\cos(\phi_n) + \cos(\phi_{n+1})] - \frac{\beta\epsilon}{r}\left[\alpha\sqrt{1 - r^2\sin^2(\phi_n)} + \sqrt{1 - r^2\sin^2(\phi_{n+1})}\right]. \tag{11}$$

We have used the Newton's method in order to solve numerically Eq. (11).

3. Numerical results: boundary crisis and the parameter-space

In this section we discuss some numerical results obtained for our variation of a dissipative FUM. In Fig. 2, we show the behavior of the invariant manifolds of two saddle fixed points (Eqs. (7) and (8)) (represented by a star for $m = 1$ and for $m = 2$) which are obtained by iteration of map T (map (1)) as well as its inverse (Eqs. (10) and (11)). Let us now discuss the behavior of the branches of the saddle point. It is easy to see in Fig. 2(a) that the two branches of the unstable manifolds evolve as follows: the upward branch generates the attracting fixed point while the downward branch creates the chaotic attractor. On the other hand, the two branches of the stable manifold, which is obtained via the iteration of the inverse mapping T (see Eqs. (10) and (11)) generate the basin boundaries for both the chaotic and the attracting fixed points. However, increasing the value of the dissipation parameter α, which is equivalent to reducing the power of the dissipation, the unstable manifold touches the stable manifold. Such a collision implies a sudden destruction of the chaotic attractor and also its basin of attraction. This sudden destruction of the chaotic attractor via a crossing of stable and unstable manifolds of the same saddle point is called a boundary crisis.

In order to illustrate this, we have obtained and characterized a boundary crisis for $m = 1$ and $m = 2$ (see Eqs. (7) and (8)), as it is shown in Fig. 2. Here we have fixed $\epsilon = 0.02$, $\beta = 0.98$ and $r = 0.5$. It is easy to see in Fig. 2(b) that already at $\alpha = 0.915$ the chaotic attractor touches the stable manifold and it is destroyed giving place to a transient. We also emphasize that before the crisis and for the combination of control parameters used in Fig. 2(a) (see details in the caption of that figure),

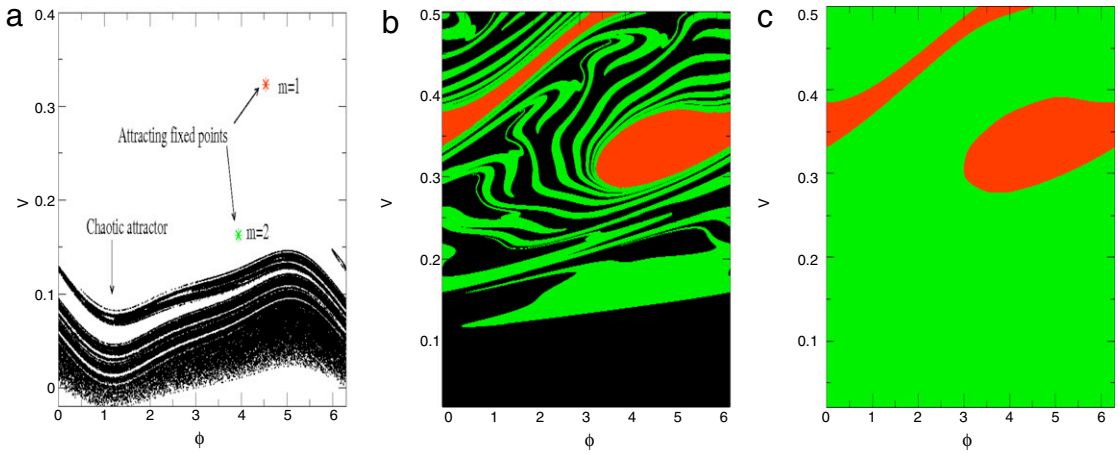

Fig. 3. (a) Attracting fixed points for $m = 1$ and $m = 2$ and a chaotic attractor. (b) Their corresponding basin of attraction. The control parameters used in (a) and (b) were $\epsilon = 0.02$, $\alpha = 0.91$, $\beta = 098$. The region in black is the basin of attraction of the chaotic attractor; the green color is the basin for the attracting fixed point for $m = 2$; in red color is the basin of attraction for the $m = 1$ attracting fixed point; (c) basin of attraction after the crisis for the attracting fixed points $m = 1$ in red and $m = 2$ in green. (For interpretation of the references to colour in this figure legend, the reader is referred to the web version of this article.)

there are three different attractors, namely: (i) two of them are attracting fixed points related to $m = 1$ and $m = 2$ and (ii) a chaotic attractor (see Fig. 3(a)). Thus one might expect there must be three different basin boundaries. This is indeed true as it is shown in Fig. 3(b). The procedure used to obtain the basin of attraction for both the chaotic and fixed point attractors consists of iterating a grid of initial conditions in the plane $V vs. \phi$ and observing their asymptotic behavior. Thus we have used a range for the initial V as $V \in [\epsilon, 0.5]$ and $\phi \in [0, 2\pi]$. Both ranges of V and ϕ were divided in 1000 parts each, leading to a total of 10^6 different initial conditions. For the combination of control parameters that we have considered, each initial condition has been iterated up to 10^5 times. Here, it is important to emphasize that the boundary crisis happens when the stable manifold touches unstable manifold of the same saddle fixed point. In our case, we have characterized a crisis for the saddle fixed point for $m = 2$. It means that every initial condition given in the region where the chaotic attractor used to be (before crisis), after a transient, will be captured by the attracting fixed point. Fig. 3(c) shows the basin of attraction of the system after the crisis. We have considered as control parameter $\epsilon = 0.02$, $\beta = 0.98$, $r = 0.5$ and $\alpha = 0.92$ and as one can see now exist two basins of attraction. One for the attracting fixed point for $m = 1$, which has the same structure as before the crisis, and all the other initial conditions, including these belonging to the chaotic attractor before the crisis, will eventually converge to the attracting fixed point for $m = 2$ and it is shown in Fig. 3(c). The procedure used to obtain Fig. 3(c) is the same applied in Fig. 3(b). We have observed that for the control parameters used in Fig. 3(b) (before crisis) 67.25% of the initial conditions belong to the basin of attraction of the chaotic attractor, 24.15% to the attracting fixed point $m = 2$ and 8.60% belong to the attracting fixed point $m = 1$. On the other hand, after the boundary crisis (Fig. 3(c)), 87.72% of the initial conditions will be captured by the attracting fixed point $m = 2$ and the other 12.28% will be attracted to the fixed point $m = 1$. Once the chaotic attractor is destroyed, these trajectories that used to form the chaotic attractor spend some characteristic time, n_t, until they leave, now, the transient and find the route to the attracting fixed point. This characteristic time, or transient, for a single initial condition can be described by a power law of the type

$$n_t = \mu^{\rho}, \tag{12}$$

where $\mu = \alpha - \alpha_c$, with $\alpha > \alpha_c$. For the combination of control parameters that we have considered, namely, $\epsilon = 0.02$, $\beta = 0.98$ and $r = 0.5$, we have found that the critical value of the dissipation parameter α is $\alpha_c = 0.9141386\cdots$. The average transient is defined by

$$\bar{n}_t = \frac{1}{B}\sum_{i=1}^{B} n_t^i, \tag{13}$$

where the index i denotes a member of an ensemble of initial conditions, and B is the number of different initial conditions. In our simulations we have considered $B = 10^4$ initial conditions randomly chosen in the chaotic attractor. Fig. 4 shows the behavior of the average transient as a function of μ, after a power law fitting we have found $\rho = -2.0(1)$, which is the same exponent obtained for the pure Fermi–Ulam model [36].

Another feature that has attracted much attention during the last decades in dissipative systems is the structure of the parameter space. To investigate the parameter space of our model we may change two control parameters, namely, the amplitude of oscillation of the moving wall ϵ and the dissipation parameter α keeping fixed the other two, namely, r and β. Additionally, as usual, in order to define whether a given region of the parameter space has chaotic or regular behavior we

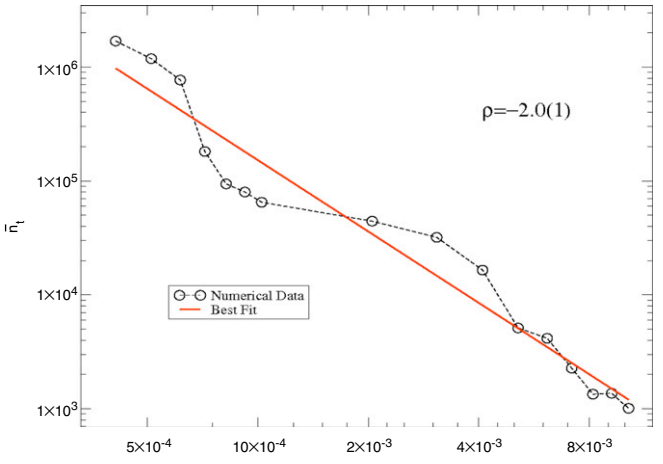

Fig. 4. Plot of $\bar{n}_t$ vs. μ. A power law fitting gives $\rho = -2.0(1)$.

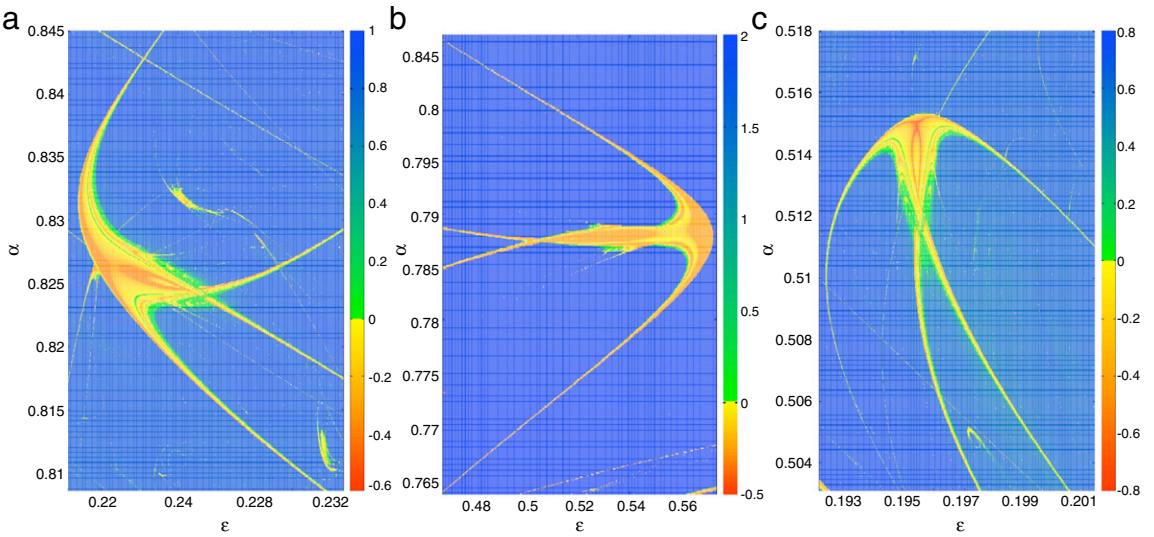

Fig. 5. Parameter-space for a dissipative Fermi–Ulam model with two nonlinearities where three shrimps are shown from different angles and considering different combinations of the control parameter. We have considered in (a) $\beta = 0.8$ and $r = 0.95$; (b) $\beta = 1$ and $r = 0.05$; (c) $\beta = 1$ and $r = 0.95$. The period of the main structures are: (a) $k = 6$, (a) $k = 3$ and (a) $k = 7$. The exponents were coded with a continuous color scale ranging from green–blue (positive exponents) to red–yellow (negative exponents). It is important to emphasize that the color scaling was normalized from plot to plot. (For interpretation of the references to colour in this figure legend, the reader is referred to the web version of this article.)

have used as a tool the Lyapunov exponents. As discussed in Ref. [37], the Lyapunov exponents are defined as

$$\lambda_j = \lim_{n\to\infty} \frac{1}{n} \ln |\Lambda_j|, \quad j = 1, 2, \tag{14}$$

where Λ_j are the eigenvalues of $K = \prod_{i=1}^{n} J_i(V_i, \phi_i)$ and J_i is the Jacobian matrix evaluated over the orbit (V_i, ϕ_i). If at least one of the λ_j is positive then the system is classified as chaotic. Let us now discuss the behavior of the parameter space. Fig. 5 shows the structure of the parameter-space for our version of the dissipative Fermi–Ulam model with two nonlinearities where a shrimp-shaped structure is evident for three different combinations of control parameters, namely, Fig. 5 (a) $\beta = 0.8$ and $r = 0.95$; (b) $\beta = 1$ and $r = 0.05$; (c) $\beta = 1$ and $r = 0.95$, where the periods of the main structures are: (a) $k = 6$, (b) $k = 3$ and (c) $k = 7$ followed by an infinite sequence of bifurcations following the rule, $k \times 2^n$. The procedure used to construct the figure was to divide both $\epsilon \in [\epsilon_i, \epsilon_f]$ and $\alpha \in [\alpha_i, \alpha_f]$ into windows of 1000 parts each, thus leading to a total of 10^6 different initial conditions, here the sub-index i denotes initial and f final, respectively. Starting with the initial condition, $\phi_0 = 3.5$ and $V_0 = 2 \times 10^{-2}$, for each increment in ϵ and α we follow the attractor, in the sense that we have used the last value obtained for (ϕ, V) before the increment, as the new pair of initial condition

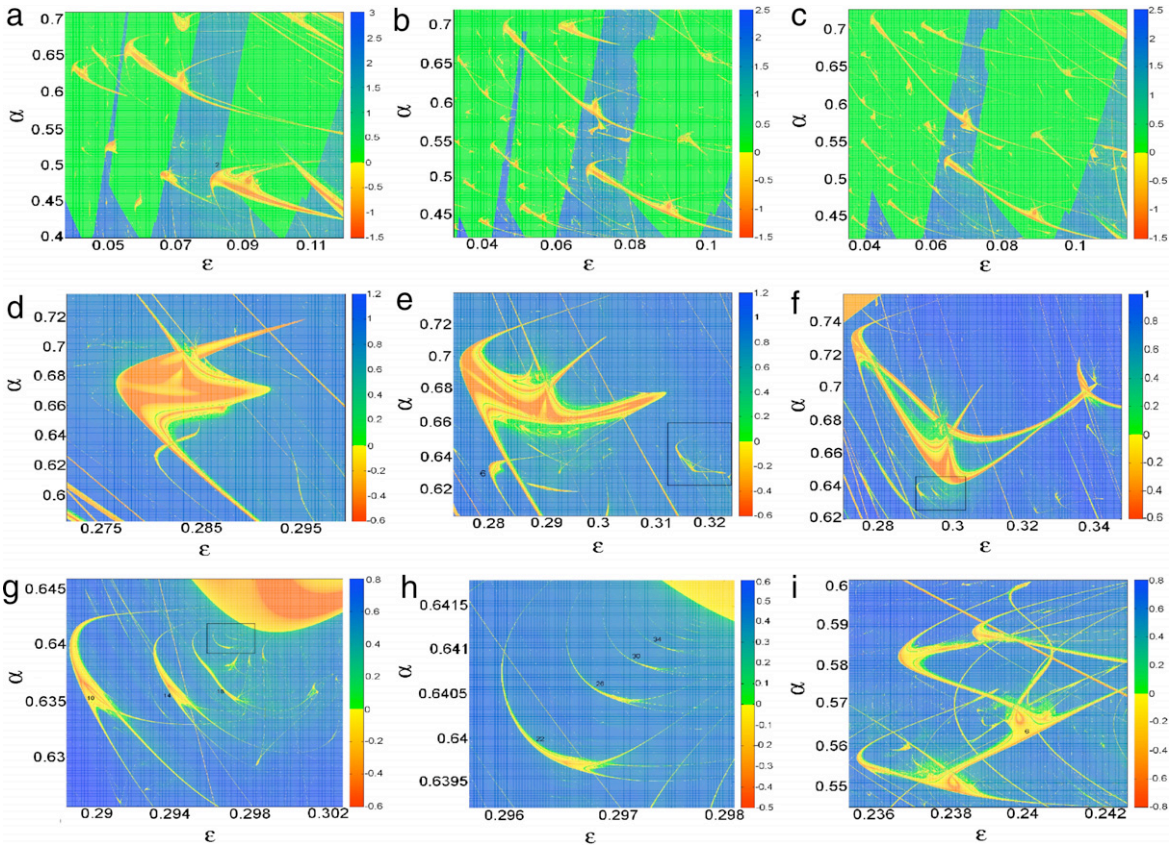

Fig. 6. The parameter space for a variant of the Fermi–Ulam model. We have considered in the first line Fig. 6 $\beta = 0.8$ and (a) $r = 0.93$, (b) $r = 0.97$ and (c) $r = 0.98$. In (d–f) we have considered $\beta = 1$ and in (d) is shown the overlap of three shrimps for $r = 0.7$ and as r increases (e) $r = 0.73$ and (f) $r = 0.76$ the shrimps become more defined. (g) is a magnification of the box in (f) and (h) is a magnification of the box in (g). (i) shows five shrimps connected by their "legs" for $\beta = 1$ and 0.8. Numbers represents the period of the main structure of each shrimp.

after the increment. However, it is possible to attribute only one color for a given combination of the control parameters (ϵ, α) in this sense we lose the information about multiple attractors. In our simulations we have considered a transient of $n = 1 \times 10^6$ iterations and we computed the Lyapunov exponent for the next $n = 1 \times 10^5$ iterations. The exponents are coded with a continuous color scale ranging from red–yellow (negative Lyapunov exponents) to green–blue (positive Lyapunov exponents). Here, it is important to emphasize that the color scaling was normalized from plot to plot in the sense that a darker blue is attributed to the most positive exponent while a lighter green for the exponent close to zero, while for negative Lyapunov exponents (red–yellow), red is attributed to more negative values and yellow is used for values of the Lyapunov exponent close to zero. Fig. 6 shows the parameter space for different combinations of the control parameters $(\alpha, \beta, \epsilon, r)$. For the figures shown in the first line we have fixed $\beta = 0.8$ and different values for r, namely, Fig. 6 (a) $r = 0.93$, (b) $r = 0.97$ and (c) $r = 0.98$. As one can see, the structures are connected, almost overlapping, forming a main and complex structure. However, as the value of the parameter r increases, the structures with shrimp-shape become more evident, and the distance between the two main bodies increases, but they are still connected by one of their "legs". Note that such a behavior is observed for all the structures in Fig. 6(a–c). This can be seen in more detail in Fig. 6(d–f) where β is assumed to be $\beta = 1$. As one can see, the structure in Fig. 6(d) is formed by the overlap of three shrimps with main period $k = 4$, and as the value of the control parameter r increases the three bodies become more evident. In this case we have considered (d) $r = 0.7$, (e) $r = 0.73$ and (f) $r = 0.76$. We would like to draw the attention to Fig. 6(e–f). Observe that the shape of the three shrimps shown in Fig. 6(f) is the same as that in the box of Fig. 6(e). Thus we conclude that changing the parameter r such a behavior might happen for other complex structures in the parameter space such as the one in Fig. 6(e) with period 6 which is still formed by the overlapping of shrimps. Here, it is important to stress that the numbers in each figure represent the period of the main structure of each shrimp. For example, Fig. 6(g) is a magnification of the box in Fig. 6(f) and Fig. 6(h) is a magnification of the box in Fig. 6(g) and it shows the infinite alternation between the structures corresponding to the chaotic and regular behavior. Starting with a shrimp with the period of the main body $k = 14$ we see that it increases by 4 ($18 \rightarrow 22 \rightarrow 26 \rightarrow 30 \rightarrow 34 \ldots$) towards another bigger periodic region (shrimp). Finally, in order to show how complex and intriguing the parameter space can be, Fig. 6(i) shows five shrimps of period 6 connected by their "legs".

4. Conclusions

We have studied a variant of a Fermi–Ulam model with two nonlinearities and we introduced dissipation due to inelastic collisions with both walls. The mapping that describes the dynamics of the system has been derived together with its corresponding inverse and we have shown explicitly via the determinant of the Jacobian matrix that the model leads to the area-contracting property. We have obtained a homoclinic crossing and thus we have shown that a boundary crisis occurs. Once the attractor has been destroyed, a chaotic transient is observed and we have shown that after crisis the transient follows a power law with exponent -2 similar as to the pure Fermi–Ulam model [36]. We have shown that varying simultaneously two control parameters, namely, the dissipation parameter α and the amplitude of the moving wall ϵ and using the Lyapunov exponents as a tool in order to classify regions of the parameter space with regular or chaotic behavior, a very rich and interesting structure has been observed with infinite self-similar periodic structures of shrimp-shape corresponding to periodic attractors, embedded in a large chaotic region which corresponds to the chaotic attractors.

Acknowledgements

DFMO gratefully acknowledges the financial support by the Slovenian Human Resources Development and Scholarship Fund (Ad futura Foundation). EDL acknowledges the financial support by FAPESP, CNPq and FUNDUNESP, Brazilian agencies. This research was supported by resources supplied by the Center for Scientific Computing (NCC/GridUNESP) of the São Paulo State University (UNESP).

References

[1] E. Fermi, Phys. Rev. 75 (1949) 1169.
[2] A.J. Lichtenberg, M.A. Lieberman, Regular and Chaotic Dynamics, in: Appl. Math. Sci., Vol. 38, Springer-Verlag, New York, 1992.
[3] D.G. Ladeira, J.K.L. da Silva, Phys. Rev. E 73 (2006) 026201.
[4] R.M. Everson, Physica D 19 (1986) 355.
[5] S.T. Dembinski, A.J. Makowski, P. Peplowski, Phys. Rev. Lett. 70 (1993) 1093.
[6] J.V. José, R. Cordery, Phys. Rev. Lett. 56 (1986) 290.
[7] P.J. Holmes, J. Sound Vib. 84 (1982) 173.
[8] E.D. Leonel, P.V.E. McClintock, J.K.L. da Silva, Phys. Rev. Lett. 93 (2004) 014101.
[9] O.F. de Alcantara Bonfim, Phys. Rev. E 79 (2009) 056212.
[10] P. Seba, Phys. Rev. A 41 (1990) 2306.
[11] M.E. Flatte', M. Holthaus, Ann. Phys. NY 245 (1996) 113.
[12] T. Dembin'ski, A.J Makowski, P. Peplowski, Phys. Rev Lett. 70 (1993) 1093.
[13] F. Saif, I. Bialynicki-Birula, M. Fortunato, W.P. Schleich, Phys. Rev. A 58 (1998) 4779.
[14] F. Saif, I. Rehman, Phys. Rev. A 75 (2007) 043610.
[15] A.J. Lichtenberg, M.A. Lieberman, R.H. Cohen, Physica D 1 (1980) 291.
[16] E.D. Leonel, M.R. Silva, J. Phys. A 41 (2008) 015104.
[17] E.D. Leonel, P.V.E. McClintock, J. Phys. A 38 (2005) L425.
[18] C. Grebogi, E. Ott, J.A. Yorke, Phys. Rev. Lett. 48 (1982) 1507.
[19] C. Grebogi, E. Ott, J.A. Yorke, Physica D 7 (1983) 181.
[20] V. L'vov, A. Pomyalov, I. Procaccia, V. Tiberkevich, Phys. Rev. Lett. 92 (2004) 244503.
[21] G. Katz, M.A. Ratner, R. Kosloff, Phys. Rev. Lett. 98 (2007) 203006.
[22] D.F.M. Oliveira, E.D. Leonel, Physica A 389 (2010) 1009.
[23] E.D. Leonel, P.V.E. McClintock, J. Phys. A 39 (2006) 11399.
[24] D.G. Ladeira, E.D. Leonel, Phys. Rev. E 81 (2010) 036216.
[25] E.D. Leonel, L.A. Bunimovich, Phys. Rev. Lett. 104 (2010) 224101.
[26] D.F.M. Oliveira, M. Robnik, Phys. Rev. E 83 (2011) 026202.
[27] J.A.C. Gallas, Phys. Rev. Lett. 70 (1993) 2714.
[28] J.A.C. Gallas, Appl. Phys. B 60 (1994) S203.
[29] J.A.C. Gallas, Physica B 202 (1994) 196.
[30] B.R. Hunt, J.A.C. Gallas, C. Grebogi, J.A. Yorke, H. Koçak, Physica D 129 (1999) 35.
[31] C. Bonatto, J.C. Garreau, J.A.C. Gallas, Phys. Rev. Lett. 95 (1–4) (2005) 143905.
[32] C. Bonatto, J.A.C. Gallas, Phys. Rev. Lett. 101 (1–4) (2008) 054101.
[33] H.A. Albuquerque, R.M. Rubinger, P.C. Rech, Phys. Lett. A 372 (2008) 4793.
[34] A. Celestino, C. Manchein, H.A. Albuquerque, M.W. Beims, Phys. Rev. Lett. 106 (2011) 234101.
[35] R. Stoop, P. Benner, Y. Uwate, Phys. Rev. Lett. 105 (1–4) (2010) 074102.
[36] E.D. Leonel, R.E. de Carvalho, Phys. Lett. A 364 (2007) 475.
[37] J.P. Eckmann, D. Ruelle, Rev. Modern Phys. 57 (1985) 617.